



HAL
open science

Thermodynamics and structural properties of CaO: A molecular dynamics simulation study

Cecilia M.S. Alvares, Guillaume Deffrennes, Alexander Pisch, Noel Jakse

► **To cite this version:**

Cecilia M.S. Alvares, Guillaume Deffrennes, Alexander Pisch, Noel Jakse. Thermodynamics and structural properties of CaO: A molecular dynamics simulation study. *The Journal of Chemical Physics*, 2020, 10.1063/1.5141841 . hal-03020747

HAL Id: hal-03020747

<https://hal.science/hal-03020747v1>

Submitted on 24 Nov 2020

HAL is a multi-disciplinary open access archive for the deposit and dissemination of scientific research documents, whether they are published or not. The documents may come from teaching and research institutions in France or abroad, or from public or private research centers.

L'archive ouverte pluridisciplinaire **HAL**, est destinée au dépôt et à la diffusion de documents scientifiques de niveau recherche, publiés ou non, émanant des établissements d'enseignement et de recherche français ou étrangers, des laboratoires publics ou privés.

Thermodynamics and structural properties of CaO: A molecular dynamics simulation study

Cecilia M. S. Alvares, Guillaume Deffrennes, Alexander Pisch, and Noël Jakse

*Univ. Grenoble Alpes, CNRS,
Grenoble INP, SIMaP,
F-38000 Grenoble, France*

(Dated: January 30, 2020)

Abstract

A detailed theoretical study of CaO in the solid and liquid states by means of combined classical and *ab initio* molecular dynamics simulations is presented. Evolution of the specific heat capacity at constant pressure as a function of temperature is studied and the melting temperature and enthalpy of fusion are determined. It is shown that an empirical Born-Mayer-Huggins potential gives a good representation of pure CaO in the liquid and solid state as compared to available experimental data and density functional theory calculations. Consistency of the predicted results obtained for CaO with data available in commercial thermodynamic databases and experimental values in the literature is discussed. The present methodology and theoretical results provide a new accurate basis for calculations of thermodynamic properties in a temperature range that is hardly accessible by experiments.

`email: noel.jakse@grenoble-inp.fr`

I. INTRODUCTION

Calcium oxide with its common mineral name - lime - is one of the key components in various scientific fields and technical applications. A non-exhaustive list includes geochemistry, ceramics and building materials as well as CO₂ capture and sequestration. Reliable thermodynamic properties up to very high temperatures are mandatory in order to be able to calculate the stability and the driving forces for the formation of CaO-bearing compounds in a given field or application.

The heat capacity at constant pressure, C_P ,¹⁻³ and the heat content $H(T) - H(298K)$ ⁴⁻¹¹ of solid CaO were measured in the past using various calorimetric techniques and data are available in the literature up to temperatures as high as 3000 K. The agreement between the different datasets is generally satisfactory. In addition, the thermal expansion was derived from high temperature diffraction experiments¹², elastic properties determination and Gamma attenuation measurements. The lattice dynamics was also studied by triple axis neutron spectrometry¹³ and phonon dispersion relations were established in three symmetry directions. The main experimental difficulty in all these measurements lies in obtaining a lime sample of high purity. CaO is generally synthesized by thermal decomposition of high purity calcite CaCO₃ or portlandite Ca(OH)₂ at medium temperatures (< 900 °C) followed by a high temperature sintering step (> 1500 °C). The obtained sample is pure but highly reactive towards CO₂(g) and H₂O(g) so that avoiding any carbonation or hydration of the sample surface is hard. In addition, if the sintering temperature is too high, vaporization is observed, leading to samples of lower density, for instance the sample used in the heat capacity measurements by Gmelin³ had a density 30% lower than the theoretical value.

The thermodynamic properties of liquid CaO were never determined experimentally due to a very high melting point and the resulting high vapor pressures of Ca(g), CaO(g) and O₂(g). The only available experimental information is the melting point of CaO. However, even this characteristic temperature was a matter of debate for quite a while as the available values in the literature varied from 2843 K¹⁵ to up to 3223 K¹⁷. Such a discrepancy of almost 400 K in the measurements is rather rare. It is now well established that the higher values, obtained in a crucible free environment either in a solar furnace^{16,17} or more recently by laser melting on a levitated sample¹⁸, might be the reliable ones. The lower value is generally discarded in view of the reaction of lime with the tungsten crucibles used. As a matter of

fact, it corresponds to a lime-lime tungstate eutectic rather than to the true melting point of pure lime. For a complete review of the available data and discussion of the selected value the recent publication by Liang and Schmid-Fetzer can be recommended¹⁹. No experimental value is available for the heat of fusion or the heat capacity at constant pressure above the melting point of liquid CaO. In the JANAF compilation¹⁴, the heat of fusion was estimated to be close to 24.88 J/molK at the melting point. By assuming a melting point of 3222 K, as suggested by Liang and Schmid-Fetzer, this leads to a value of 80.2 kJ/mol. Using a different approach, Chang and Howald²⁰ evaluated a heat of fusion of 57.65 ± 8 kJ/mol from the slope of the liquidus in the CaO-MgO phase diagram, which is considerably lower than the JANAF one. Another estimation is necessary for the heat capacity at constant pressure C_P of liquid CaO as there is no experimental data available for this thermodynamic property. A high temperature value of 62.76 J/molK is recorded in the JANAF tables by taking 2/3 of the melting temperature as a common rule for the fictive glass transition temperature, namely 2100 K. Another possibility to derive the heat capacity is to accept C_P data for CaO as a compound of liquid or glassy binary system, and assume the validity of Neumann and Kopp's additive rule to subtract the contribution from the other constituent oxides. Using the experimental values for liquid Wollastonite CaSiO_3 ²¹ a value range of 80 to 86 J/molK is obtained for C_P above 1500 K. This value is 30% higher than the one in the JANAF compilation. A third estimation was reported in Gurvich's compilation²², with a value of 84 ± 10 J/molK obtained by comparing with the heat capacity of BeO(l) and BaO(l).

In this context, atomistic calculations based on the Density Functional Theory (DFT)²³ and Molecular Dynamics (MD) simulations^{24,25} represent a powerful way of generating high quality thermodynamic data. The heat capacity of crystalline CaO at low temperatures can be obtained very accurately from DFT calculations using the quasi-harmonic approximation, while for higher temperatures as well as for the liquid phase, MD is the dedicated method. In DFT calculation, the General Gradient Approximation (GGA) is commonly used, but it is known that this functional overestimates the lattice parameters. In addition, the heat of formation cannot be derived directly from the calculations and corrections often have to be applied. The results generally improve when using hybrid or meta-GGA functionals, and the best predictions are obtained with the recently developed Strongly Constrained and Appropriately Normed (SCAN) functional. Only few MD simulations for liquid CaO were reported in the literature so far, either using *ab initio* MD (AIMD)²⁶ or classical MD with

empirical potentials^{27–29}, and often studied as a limiting case component of a binary liquid such as CaO-SiO₂, CaO-CaF and CaO-BaO, or ternary liquids like MgO-CaO-SiO₂³⁰ and CaO-Al₂O₃-SiO₂^{31–33}. Interactions in classical MD are taken in the form of a Born-Mayer (BM) or Born-Mayer-Huggins (BMH) type³⁵ which are generally suitable for oxides³⁴.

The purpose of this contribution is to present a detailed theoretical study of solid and liquid CaO by means of combined *ab initio* and classical MD simulations. Additional static DFT calculation were performed to determine the temperature evolution of C_P within the lattice dynamics theory³⁷ in the crystalline states at low temperatures. Classical MD were performed using a BMH empirical potential^{31–33} to determine the temperature evolution of the enthalpy, constant pressure specific heat as well as the melting temperature and related enthalpy of fusion. Our findings indicate that the empirical Born-Mayer-Huggins potential used^{31–33} gives an adequate representation of pure CaO in the liquid and solid states as compared to available experimental data and DFT. The present methodology and theoretical results provide an new accurate basis for thermodynamic calculations, and results are discussed within the calculation of phase diagrams³⁹ (CALPHAD) framework.

II. SIMULATION BACKGROUND

A. Density Functional Theory

Density functional theory^{40,41} calculations were performed in order to: (i) obtain the ground state properties of solid CaO and (ii) carry out *ab initio* molecular dynamic simulations in the solid and liquid state at finite temperatures for selected states. The Vienna *ab initio* simulation package (VASP)^{42,43} in its most recent release (5.4.4) was used. The projected augmented-wave method^{44,45} was used to describe the electron-ion interactions together with recently developed Strongly Conditioned and Appropriately Normed (SCAN) many-body exchange correlation functional³⁶. For Ca, the 3s3p4s orbitals and for O the 2s2p orbitals were considered as valence states with a cut-off energy set to 800 eV. The Γ -centered grid of k -points in the irreducible part of the Brillouin zone was set to $11 \times 11 \times 11$ and automatically generated following the Monkhorst-Pack scheme⁴⁶. For liquid state calculations, we kept only the Γ point. The lattice parameters at 0 K were fully relaxed and the linear tetrahedron method with Blöchl corrections⁴⁷ was used to calculate the electronic density of

states (DOS). The relaxations were performed with a convergence criterion of 10^{-8} eV/Å for the total energy.

Within the DFT, finite temperature properties such as the Helmholtz free energy F and heat capacities at constant volume, C_V , or pressure C_P were obtained through the lattice dynamics theory³⁷. The phonon spectrum of CaO was determined using the frozen phonon supercell method, and the vibrational modes were calculated using the phonopy code⁴⁸ coupled to VASP. The convergence criteria for the Hellman-Feynman forces was set to 10^{-6} eV/Å to avoid any residual strain in the lattice and a $3 \times 3 \times 3$ supercell was generated for the calculations.

Within the Harmonic Approximation (HA), the Helmholtz free energy F at constant volume is written in terms of their phonon density of states as a function of frequency q of the band s as

$$F(V_0, T) = \underbrace{\frac{1}{2} \sum_{\mathbf{q}, s} \hbar \omega(\mathbf{q}, s)}_{\text{ZPE}} + k_B T \sum_{\mathbf{q}, s} \ln \left[1 - \exp \left(-\frac{\hbar \omega(\mathbf{q}, s)}{k_B T} \right) \right], \quad (1)$$

while the heat capacity at constant volume takes the following expression

$$C_V = -T \left(\frac{\partial^2 F}{\partial T^2} \right)_V. \quad (2)$$

Then by using quasi-harmonic approximation (QHA), that is repeating the HA calculation at several volumes V to get the minimum of $F(V, T)$, the heat capacity at constant pressure is derived from

$$C_P(T, P) = -T \frac{\partial^2 G(T, P)}{\partial T^2} \quad (3)$$

with

$$G(T, P) = \min_V [E(V) + F(V; T) + PV]. \quad (4)$$

B. Molecular Dynamics Simulations

We have first performed AIMD simulations using the VASP code in the same conditions than the static calculations described above, in order to assess the classical MD simulations. The dynamics was performed in the canonical ensemble, namely constant number of atoms, volume, and temperature (NVT) by means of a Nosé thermostat^{24,25}. Newton's equations of motion were integrated using Verlet's algorithm in the velocity form with a time step of 1 fs.

Cubic simulation supercells with periodic boundary conditions containing 216 atoms were used. Simulations were performed in the solid state at high temperatures, *i.e.* at $T = 300$ K, $T = 1500$ K, $T = 2500$ K, and $T = 3000$ K. The volume of the simulation box was adjusted to reach the ambient pressure for each temperature. Another simulation was carried out in the liquid state at $T = 3200$ K in the vicinity of the melting point.

For the simulation in the solid state, an initial relaxed crystalline configuration in the B2 structure, obtained from the static calculation described above, was progressively heated from 0 K to the target temperature and then the volume was adjusted to get the ambient pressure. After an equilibration period of 20 ps, runs were subsequently continued for another 60 ps during which the properties were extracted from a statistical analysis. The system was progressively heated again up to 3500 K where a complete melting was observed. The obtained liquid was then cooled down to 3200 K. The volume of the simulation box was adjusted to get the ambient pressure and the same procedure as in the solid state was followed for equilibration and calculation of the liquid state properties.

Secondly, we have performed classical MD simulations using atomic interactions chosen in the form of the Born-Mayer-Huggins potential³⁵ for which interactions between Ca and O atoms are given⁴⁹ by

$$u(r_{ij}) = \frac{q_i q_j}{r_{ij}} + A_{ij} \exp\left(\frac{\sigma_{ij} - r_{ij}}{\rho_{ij}}\right) - \left(\frac{C_{ij}}{r_{ij}}\right)^6 - \left(\frac{D_{ij}}{r_{ij}}\right)^8, \quad (5)$$

with i and $j = \text{Ca}$ and O and r being the interatomic distance between two ions of species i and j . It should be noted that in the dipolar expansion only the van der Waals term was taken into account. Parameters in Eq. (5) are given in Table I and readily taken from the potentials used successfully to describe the calcium aluminosilicate (CAS) ternary system^{50,51}, and the aluminosilicate (AS) binary⁵³ proposed recently by Bouhadja *et al.*³¹⁻³³.

Using this empirical potential classical molecular dynamics simulations were performed with the LAMMPS code⁵². The number of atoms in the simulation box was set to 1620 with an initial crystalline configuration. Periodic boundary conditions were applied in the three directions of space, and the long-range Coulomb interactions were treated within the Ewald summation method²⁴. Equations of motion were solved numerically within the Verlet algorithm in the velocity form^{24,25} using a time step of 1 fs. All simulations were performed in the isobaric-isothermal ensemble (NPT) with ambient pressure using a Nose-

	q	A (eV)	ρ (Å)	σ (Å)	C (eVÅ ⁶)
Ca	1.2				
O	-1.2				
Ca-Ca		0.0035	0.0800	2.3440	20.9856
Ca-O		0.0077	0.1780	2.9935	42.2556
O-O		0.0120	0.2630	3.6430	85.0840

TABLE I: Parameters for the CaO potential taken from preceding works³¹⁻³³ (see Eq. 5).

Hoover thermostat and barostat²⁴.

In the general case, a first stage consists in equilibrating the system for 100 ps at the desired temperature followed by a production run of 200 ps. For the temperature evolution of the properties in the solid state, a first simulation is run at 300 K and the subsequent higher temperatures were reached step-wise with a temperature step of 50 K at the end of each simulation. For the liquid state, before equilibration, a progressive heating stage is performed at 10^{12} K/s to 4000 K to get a fully melted configuration. Then, the system was cooled down stepwise with the same temperature step as for the the solid branch and we stopped this process when crystallization is observed. It should be mentioned that quenching runs were also carried out with various cooling rate ranging from 10^{11} K/s to 10^{13} K/s, to observe the glass transition. However, the latter was never observed as the system crystallized during cooling around $T = 2100$ K whatever the cooling rate.

In order to test the reliability of the BMH potential in the liquid state, the partial pair-correlation functions $g_{ij}(r)$, giving the probability of finding a particle j at distances r relative to a particle i located at the origin, were considered:

$$g_{ij}(r) = \frac{N}{V} \frac{n_{ij}(r)}{4\pi r^2 \Delta r}. \quad (6)$$

$n_{ij}(r)$ represents the mean number of particles j in a spherical shell of radius r and thickness Δr centered on particle i . Integrating $g_{ij}(r)$ up to their first minimum gives access to the partial coordination numbers.

Concerning the dynamics, we determined the self-diffusion coefficient D_i of each species

from the linear behavior at long times of the mean-square displacement

$$R_i^2(t) = \frac{1}{N} \sum_{l=1}^{N_i} \left\langle [\mathbf{r}_l(t+t_0) - \mathbf{r}_l(t_0)]^2 \right\rangle_{t_0}, \quad (7)$$

where $\mathbf{r}_l(t)$ denotes the position of atom l at time t and N_i is the number of particles of specie i . As for the short-time dynamics, we have considered the velocity auto-correlation function (VACF) :

$$\Psi(t) = \frac{1}{N} \left\langle \sum_{i=1}^N [\mathbf{v}_i(t+t_0) \cdot \mathbf{v}_i(t_0)]^2 \right\rangle_{t_0}, \quad (8)$$

where $\mathbf{v}_i(t)$ denotes the velocity of atom i at time t . The angular brackets correspond to an averaging over time origins t_0 .

In MD simulations, the enthalpy is directly calculated from positions and velocities during the simulation.

$$H(P, T) = \frac{1}{2} \sum_{i=1}^N m_i \mathbf{v}_i^2 + \frac{1}{2} \sum_{i<j=1}^N u(r_{ij}) + P_{ext} V, \quad (9)$$

where P_{ext} is the pressure imposed to the simulation box, and the volume V is a dynamical variable. The heat capacity at constant pressure C_P was determined from the numerical derivative of the enthalpy as

$$C_P(T, P) = \frac{\partial H(T, P)}{\partial T} \quad (10)$$

The estimation of the enthalpy difference at melting requires the determination of the thermodynamic melting temperature. For a given interaction model, the latter could be obtained directly from MD simulation by heating up a solid state and observe dynamically the melting. However, it is well known that for a perfect crystal this leads to a melting occurring at a considerably higher value than the thermodynamic melting temperature due to finite size effects. Avoiding these super-heating effects requires the use of specific techniques such as the direct simulation of the solid-liquid interface⁵⁴ or void-nucleated melting techniques^{55,56}. As in our preceding work⁵⁷, the method proposed by Solca *et al.*⁵⁸ was used, in which a void is created in the crystal by removing an atom as well as a certain number n of its neighbors to nucleate the melting, recalling that a single Schottky defect is known to be insufficient to induce melting at the thermodynamic melting temperature. This method was applied successfully to various systems by Agrawal *et al.*⁵⁶.

The procedure of such a void-melting simulations consist in creating single void of n atoms in a relaxed crystalline configuration at the center of the simulation box. The system

is then heated up by applying a heating rate $T = 10^{12}$ K/s. The energy is monitored during the simulation and the melting is observed from a sharp increase of the enthalpy. This heating is repeated for increasing values of n from 0, which correspond to the perfect crystal situation, to the so-called critical size where the crystal destabilizes at low temperatures. All MD simulations were performed in the NPT ensemble.

III. RESULTS AND DISCUSSION

A. Structure and diffusion in the liquid state

In a first stage, the reliability of the BMH potential is tested against *ab initio* calculations in the liquid, as no experimental data exist in the literature, to the best of our knowledge. As mentioned in the preceding Section, AIMD simulations for liquid CaO were performed at $T = 3200$ K with the volume adjusted to get ambient pressure. To make the comparison reliable, MD simulations with the same density and same temperature were executed. The partial pair-correlation functions, $g(r_{ij})$, from AIMD and MD are compared in Fig 1. Agreement is found for the three partials, indicating that the chemical ordering is well reproduced. As expected a strong Ca-O bond is seen and the Ca-Ca and O-O partials show a similar shape. The resulting partial coordination numbers are $N_{\text{Ca-Ca}} = 6.9$, $N_{\text{Ca-O}} = 2.0$, and $N_{\text{O-O}} = 6.9$, giving a average coordination number of 8.9. However, with respect to the AIMD results, the BMH potential gives a stronger Ca-O bonding and the height of the first peak of Ca-Ca partial less pronounced. It is worth noting that imposing the density obtained in the AIMD simulation to the classical one resulted in an increase of pressure up to 1.31 ± 0.4 GPa. Thus, an additional MD simulation was performed at ambient pressure, and indeed an increase of the volume of the simulation box by 5.6% was observed, as it will be seen in Fig. 4 below. Nevertheless, the corresponding pair-correlation functions, denoted by the dashed curves, are only slightly affected by such a change of the volume.

Another stringent test of the BMH potential is the dynamics. In Fig. 2, the velocity auto-correlation functions, normalized to their value at time $t = 0$, $\Psi(t = 0)$, are drawn for each species. Both AIMD and MD show similar features with a negative well at short time, characteristic of a back-scattering effect due to the first neighbor atoms' cage, followed by a rapid damping towards zero, attesting the relaxation of the system on the sub-picosecond

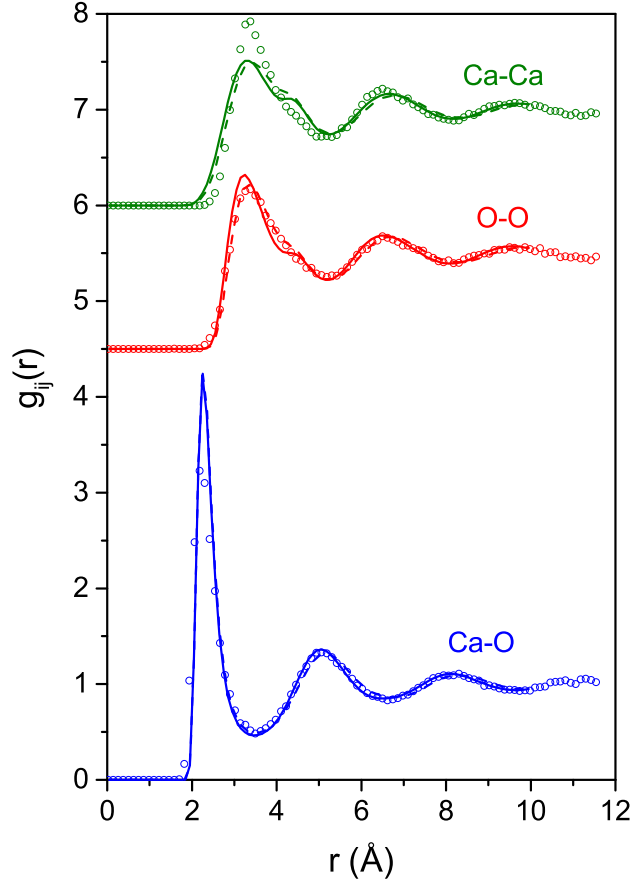


FIG. 1: Pair-correlation function of Liquid CaO at $T = 3200$ K. Symbols and lines correspond to *ab initio* and classical molecular dynamics simulations, respectively. The solid line stems from the DM simulation with the imposed *ab initio* volume, while the dashed lines correspond to the simulation at ambient pressure (see text). The curve for O-O and Ca-Ca are shifted upwards by an amount of 4.5 and 6 for the sake of clarity.

time scale. The back-scattering is more pronounced for the *ab initio* calculations, due to the stronger bonding properties seen on $g_{ij}(r)$. However, this has essentially no consequences on the diffusion at longer time scale, as can be seen on the mean-square displacement in the inset of Fig. 2. The long time behavior of $R^2(t)$ is linear, which is a characteristic feature of the liquid state. The self-diffusion coefficients, D_{Ca} and D_{O} of Ca and O, respectively, can be extracted from the long-time slope of the corresponding of $R^2(t)$. For the MD simulation

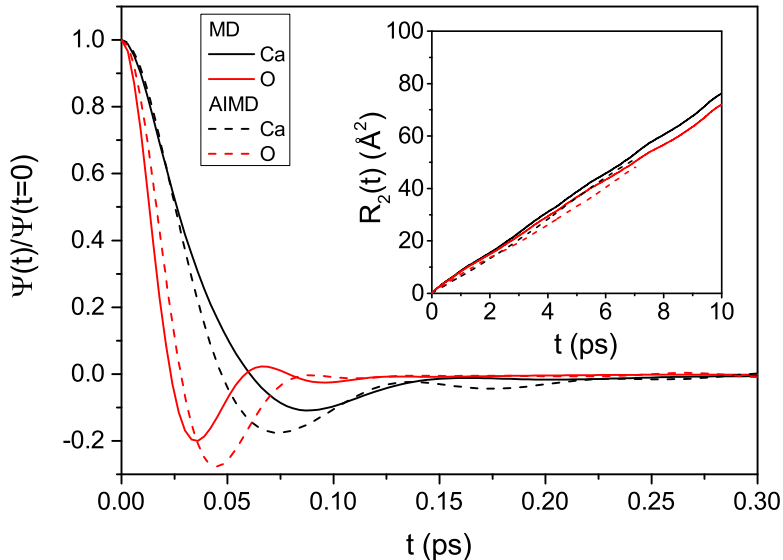


FIG. 2: Velocity auto-correlation function of Ca and O atoms in liquid CaO at $T = 3200$ K. Inset: Corresponding mean-square displacement.

$D_{\text{Ca}} = 1.31 \pm 0.05$ Å/ps and $D_{\text{O}} = 1.21 \pm 0.05$ Å/ps, which are in good agreement with the AIMD values, *i.e.*, $D_{\text{Ca}} = 1.22 \pm 0.1$ Å/ps and $D_{\text{O}} = 1.17 \pm 0.1$ Å/ps. Finally, from the results of Figs. 1 and 2 for the atomic structure and diffusion, the BMH potential gives a reasonable description of liquid CaO, as compared with the DFT calculations.

B. Enthalpy and melting temperature

The enthalpy curves of CaO at ambient pressure for the solid and liquid branches were determined by MD simulation using the BMH potential, and are plotted in Fig. 3(a) with respect to the reference value at $T = 300$ K. The simulation is started at $T = 300$ K with a perfect crystal and $N = 5832$ atoms. A NPT simulation is performed during 300 ps (100 ps equilibration and 200 ps production) and followed by a step-wise heating with a temperature step of 50 K. The procedure is repeated until a dynamic melting is observed in the simulation box, which occurred at $T = 3500$ K. The average value of the enthalpy is calculated from the production stage and the error bars are evaluated from the standard deviation of the Gaussian distribution. For the liquid branch, the MD simulations are started at $T = 4000$ K with a disordered initial configuration of $N = 1620$ atoms. The same procedure as for

the solid branch is followed but with a step-wise cooling down to 2050 K, where a partial crystallization is detected. It is worth mentioning that above $T = 3500$ K, the difference in the enthalpy from the heating and cooling process is negligible indicating that neither size effects nor reminiscence from the crystal exist.

The calculated enthalpy of the solid branch by MD is found to be in excellent agreement with experimental data⁴⁻¹⁰ below 1500 K, as well as with AIMD and DFT-QHA calculations. As can be seen, the latter gives good results up to temperatures as high as 1500 K. Above, the DFT-QHA underestimates the AIMD. This confirms earlier findings^{37,38} showing that for oxides the QHA can be generally extended up to significantly high temperatures, anharmonic contributions being small if only high symmetry positions are present as it is the case for CaO.

At higher temperatures, the MD simulated data overestimate measurements, with a departure not exceeding 11% near the melting point at 3000 K. AIMD values at 2500 K and 3000 K, are higher than the experimental data by about 3%. The observed difference between the calculated and experimental values can at least partly be explained by the experimental difficulty to obtain reliable measured data. In the very high temperature measurement above 2000 K, reaction with the crucible material is observed together with vaporization¹¹. In addition, the exact determination of the temperature is tricky and uncertainties of 20 K are frequently observed. Therefore, we estimate the uncertainty of the measurement of at least 3 – 5% at very high temperature and 1 – 3% in the temperature interval from room temperature to 2000 K. As for the liquid branch, the value of the enthalpy obtained by MD is in good agreement with the AIMD with a difference of 5%, given the experimental uncertainty. The good agreement of MD results with AIMD and experiments allows us to infer reliable values of the enthalpy at melting discussed below as well as the specific heat for the liquid and solid states presented in Section III D.

Determination of the enthalpy of melting from the liquid and solid branches obtained by MD, requires, however, the precise determination of the thermodynamic melting temperature of the BMH potential. The latter was inferred from the void-melting technique described in Sec. II. To this end, the heating procedure used to determine the solid branch of the enthalpy, with the same number of atoms ($N = 5832$) and a temperature step of 10 K, practicing in addition single cubic voids of various sizes. Fig. 3(b) shows the evolution of the melting temperature as a function of void size. It displays clearly a plateau for which

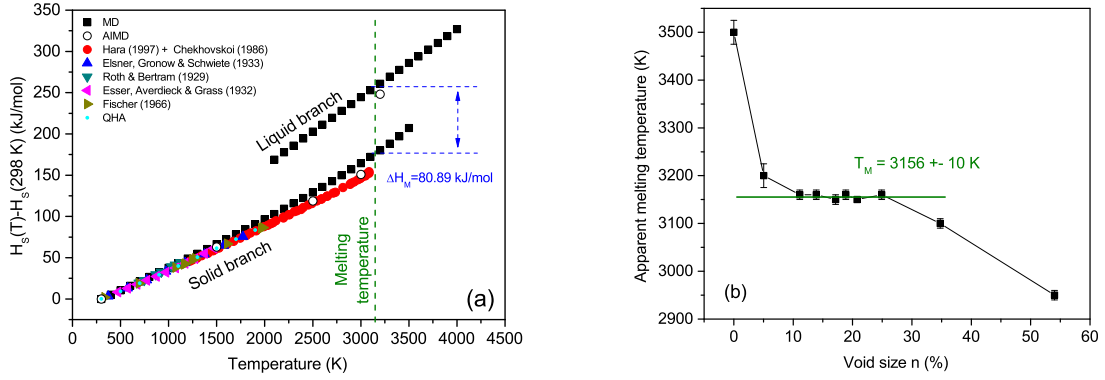


FIG. 3: (a) Enthalpy as a function of temperature for the solid and liquid state from classical MD simulations. (b) Apparent melting temperature as a function of the volume of the void (in % of the simulation box volume).

the melting temperature remains steady with the void size. Taking the obtained values between 9 and 27%, an average melting temperature of $3156 \pm 10\text{ K}$ is found. As discussed above, the values found in the literature span over 400 K. Our value is located in the range between 3128 K and 3228 K corresponding to experimental measurements of Foex^{16,17} and Manara *et al.*¹⁸ and confirm that reported temperature data around 2843 K are too low and should be discarded. It is worth mentioning that the MD value obtained by Seo *et al.*^{27,28} ($3210 \pm 10\text{ K}$) is higher than the one determined here. However, their value was inferred from a dynamic melting of the crystal which might lead to an overestimation of several hundred of K in their obtained thermodynamic melting temperature. Finally, taking the enthalpy difference between the liquid and solid branches at 3156 K yields the values of 80.89 kJ/mol. The resulting entropy of fusion of 25.6 J/molK agrees well with the estimations from the JANAF¹⁴ and Gurvich²². The estimated data from Chang and Howald⁵⁹ can therefore be discarded. As their value is derived from phase diagram studies, this would indicate that the underlying experimental data may be doubtful. This is not a surprise as the measurements at high temperature are difficult and reaction with crucibles can hardly be avoided, as can be seen from the dispersion in the melting point of CaO.

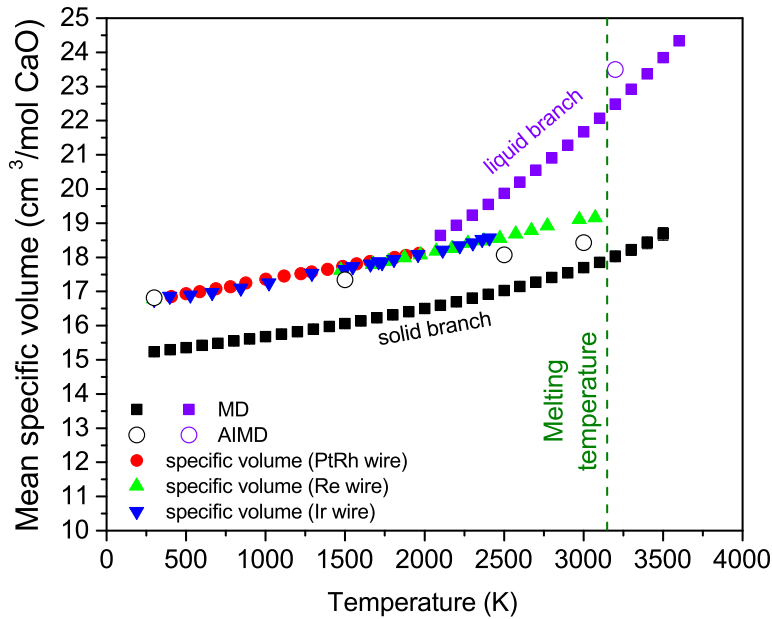


FIG. 4: Specific volume for solid and liquid CaO as a function of temperature.

C. Specific volume

Figure 4 displays the evolution of the specific volume with temperature for the solid and liquid branches at ambient pressure. For the solid branch, our MD results are compared with experimental data¹² and AIMD values. The MD simulation underestimates the experimental specific volume by about 10% whatever the temperature. This discrepancy results in a departure of the lattice parameter of 3%, which is the main drawback of the BMH potential. The AIMD reproduce quite nicely the experiment, especially at ambient temperature and, near the melting point, an underestimation of only 3% is seen. This indicates the high quality of the SCAN approach in describing the exchange and correlation effects in the DFT. For the liquid branch, the specific volume obtained by MD underestimates the AIMD one by 1.5%, which is consistent with what has been observed in Section III A for the determination of structural properties.

While changing the volume in the MD simulations to the *ab initio* one has only a little influence on the local structure, as was shown in Section III A, it could affect more significantly the enthalpy and the enthalpy of melting. More specifically, the difference of specific volume of about 10% in the solid state could affect significantly these quantities. In order to

highlight this effect, additional MD simulations at 300 K and 2973 K at constant volume with the experimental value of the specific volume were performed. The increase of the volume by 10% results in a change of the enthalpy by only 9% when approaching melting. This is also the case for the MD simulation in the liquid, and consequently only a negligible change in the enthalpy of melting is seen. Therefore the value obtained with the BMH potential can be considered as robust.

D. Heat capacity at constant pressure

We come now to the determination of the specific heat at constant pressure, C_P , which was inferred from the values of the enthalpy obtained by MD, using Eq. (10) exploited numerically by performing a local centered finite difference. Figure 5 shows the temperature evolution of C_P for the solid and liquid branches. For the solid branch, results are compared to DFT-QHA calculations, and with experimental data inferred numerically from the enthalpy differences. Our DFT-QHA values are in good agreement with the experiment up to 1500 K, given the experimental uncertainties. It is worth mentioning that the SCAN functional used in the present work perform better than the standard LDA and GGA as well as hybrid functionals for solid CaO⁶⁰. The values of C_P obtained by MD are in good agreement with DFT-QHA, up to 1200 K. Obviously, below 500 K, the classical simulations are not expected to capture the quantum behavior of C_P . For the liquid branch, the C_P is almost flat in the vicinity of the melting temperature and shows an increase with decreasing temperature in the undercooled region, as expected^{61,62}.

As there is no experimental data available for the C_P in the liquid phase, our calculated values can be compared to the CALPHAD results available in both SGTE and FACTPS databases. In these commercial databases, the data was estimated if no experimental data is available. In the case of SGTE, the value from Gurvich²² was accepted. In FACTPS, the JANAF estimation¹⁴ was preferred. Our calculated heat capacity at melting of 1.525 J/g/K is in excellent agreement with the SGTE database²² giving a value of 1.498 while the value of FACTPS, *i.e.* 1.119, is considerably lower⁶⁴. It is worth mentioning that Belmonte *et al.*⁶³ proposed recently to infer C_P of liquid CaO from a combination DFT-QHA calculations of the solid and an Anharmonic contribution issued from an analysis of the CaO melting curve added to the $3R$ value. Their results are somewhat higher than the values estimated in the

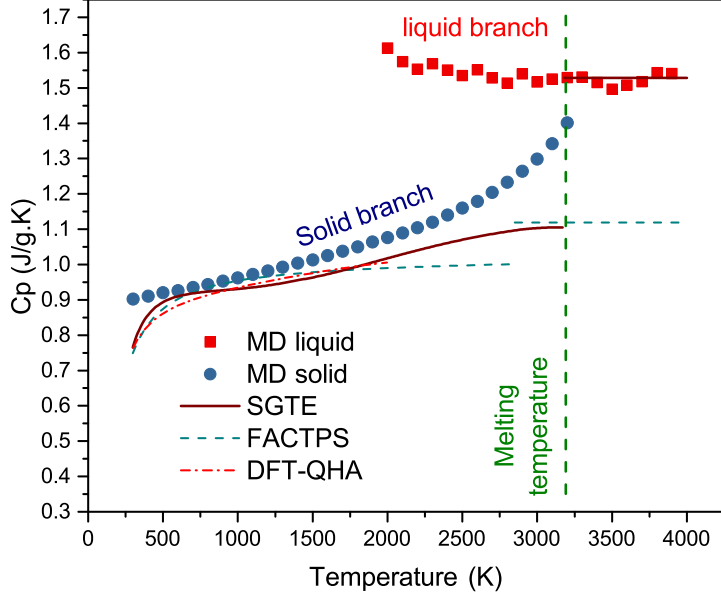


FIG. 5: Constant pressure specific heat for solid and liquid CaO as a function of temperature. Results are compared to thermodynamic calculations with DFT-QHA, SGTE, and FACTPS.

JANAF compilation but still lower than the values estimated by Gurvich *et al.*²², accepted in the SGTE pure substance database, and our MD value, despite the fact that the specific volumes obtained by MD and their approach are similar.

IV. CONCLUSION

In the present contribution, we report a detailed theoretical study of the thermodynamics of CaO in the solid state from ambient temperatures up to the melting as well as in the liquid from undercooled up to high temperature stable states. The objective was to describe evolution of the constant pressure heat capacity with temperature in the whole temperature range, and the enthalpy of melting that requires the precise determination of the melting temperature. For this purpose, combined classical and *ab initio* molecular dynamics simulations were performed.

Classical MD simulations were carried out with an empirical Born-Mayer-Huggins potential initially designed for the ternary calcium aluminosilicate system. Taking the parameters

of the potential as-such from that of the ternary system, the accuracy and transferability of the potential was first assessed in the liquid state above melting at $T = 3200$ K. In the absence of experimental data, the comparison was made with AIMD simulations using the recently developed SCAN meta-GGA functional, which improves the results over the standard LDA and GGA. It is shown that the BMH potential gives a good representation of the structure and dynamics in the liquid above the melting point with respect to AIMD.

The potential is further tested in the solid state on the enthalpy and specific volume, with existing experimental values in the whole temperature range and AIMD for some temperatures. The enthalpy calculated with the BMH is in good agreement with experimental and AIMD data below $T = 1500$ K, while progressive overestimation is seen above with increasing temperatures, with a maximum departure of 10% with measurements and 5% with AIMD around 3000 K. The specific volume obtained by classical MD underestimates the experimental data by about 10%. Nevertheless, in the vicinity of melting a reasonable agreement with AIMD is found, with a departure of 5% only. Moreover, it should be mentioned that MD simulations with imposed experimental volume gives rise to enthalpy and specific heat changes by only 2 and 5% around 3000 K, respectively. Given the experimental difficulties at high temperature near 3000 K altering the accuracy of measurements, and the good concordance with AIMD, our results reveal a reasonable transferability of the BMH potential to pure CaO in the liquid and solid states, and assures the robustness of the results presented here.

A void-melting approach yields a value of $3156 \pm -10K$ for the melting temperature of the BMH potential. Given the high diversity of the values found in the literature, our results concur with a melting temperature of CaO in the range between 3128 K and 3228 K corresponding to experimental measurements of Foex^{16,17} and Manara et al¹⁸. Our results confirm that the reported temperature values around 2843 K are too low and should be discarded. Consequently, a value for the enthalpy of melting of 80.89 kJ/mol is obtained which is consistent with the accepted estimation in the SGTE database, namely 85 kJ/mol. The corresponding entropy of fusion agrees well with the estimations in the JANAF¹⁴ and Gurvich²² compilations.

Finally, the specific heat at constant pressure obtained by MD for the solid branch is in good agreement with static DFT calculations within the quasi-harmonic approximation, at low temperatures for which the latter is valid. For the liquid branch, C_P is almost constant in

the vicinity of the melting temperature and shows an increase with decreasing temperature in the undercooled region and the value at melting is 1.498 J/g/K in excellent agreement with the SGTE database. The present methodology and theoretical results provide a new accurate basis for thermodynamic calculations with accurate predictions for temperatures hardly accessible to experiments. It has proven to be successful for solid and liquid CaO and will be extended to other compounds in future works.

Acknowledgement

We acknowledge the CINES and IDRIS under Project N INP2227/72914, as well as CIMENT/GRICAD for computational resources. This work was performed within the framework of the Centre of Excellence of Multifunctional Architected Materials "CEMAM" ANR-10-LABX-44-01 funded by the "Investments for the Future" Program. Financial support was also provided in the frame of the "OPALHE" project in the "Institut Carnot - Energie du Future" Program. Fruitful discussions within the French collaborative network in high temperature thermodynamics GDR CNRS 3584 (TherMatHT) are also acknowledged.

-
- ¹ W. Nernst, F. Schwers, S.B. *Deutsch. Akad. Wiss. Berlin* **355** (1914).
 - ² G.S. Parks, K.K. Kelly, *J. Phys. Chem* **30** 47 (1926).
 - ³ E. Gmelin, *Z. Naturforschung* **24a** 1794-1800 (1969).
 - ⁴ A. Magnus, *Phys. Ztschr.* **14** 5 (1913).
 - ⁵ W.A. Roth, I. Bertram, *Z. Elektrochem.* **35**, 296 (1929).
 - ⁶ H. Esser, R. Averdick, W. Grass, *Arch. Eisenhuettenwesen* **6**, 289 (1932-1933).
 - ⁷ H. Elsner v. Gronow, H.E. Schwiete, *Z. anorg. allgem. Chem.* **216**, 185 (1933).
 - ⁸ J.J. Lander, *J. Amer. Chem. Soc.* **73**, 5794 (1951).
 - ⁹ W.A. Fischer, W. Ertmer, *Arch. Eisenhuettenwesen* **37**, 275 (1966).
 - ¹⁰ Sh. Hara, *Goon Gaikkaishi* **23** 25 (1997).
 - ¹¹ V. Ya. Chekhovskoi, Kh. Irgashov, V.D. Tarasov, *Teplofiz. Vysok. Temp.* **24** 614 (1986).
 - ¹² G. Fiquet, P. Richet, G. Montagnac, *Phys. Chem. Min.* **27**, 103 (1999).

- ¹³ D.H. Saunderson, G.E. Peckham, J. Phys. C: Solid St. Phys. **4**, 2009 (1971).
- ¹⁴ M.W. Chase, National Institute of Standards and Technology (U.S.), eds., NIST-JANAF thermochemical tables, 4th ed, American Chemical Society; American Institute of Physics for the National Institute of Standards and Technology, Washington, DC: New York, (1998).
- ¹⁵ C.W. Kanolt, J. Wash. Acad. Sci. **3**, 315 (1913).
- ¹⁶ M. Foex, Sol. Energy **9**, 61 (1965).
- ¹⁷ M. Foex, Proc. Symp. 5, Int. At. Energy Agency, Vienne (Austria) 3139-3160 (1968).
- ¹⁸ D. Manara, R. Bohler, L. Capriotti, A. Quaini, Z. Bao, K. Boboridis, L. Luzzi, A. Janssen, P. Poml, R. Eloirdi, R.J.M. Konings, J. Eur. Ceram. Soc. **34(6)** 1623-1636 (2014).
- ¹⁹ H. Liang, R. Schmid-Fetzer J. Eur. Ceram. Soc. **38**, 4768 (2018).
- ²⁰ D.R. Chang, R.A. Howald, High Temp. Sci. **15** 209 (1982).
- ²¹ P. Richet and G. Fiquet J. Geol. Res. **49**, 445 (1991).
- ²² L.V. Gurvich, I.V. Veyts, C.B. Alcock *Thermodynamic Properties of Individual Substances*, Volume 3, CRC Press, Inc. (1994).
- ²³ J. Hafner, J. Comput. Chem. **29**, 2044 (2008).
- ²⁴ M. P. Allen, D. J. Tildesley. *Computer simulation of liquids*, Oxford Science Publication (1989).
- ²⁵ B. Smit, D. Frenkel. *Understanding molecular simulations*, 2nd ed., Academic Press, San Diego (2002).
- ²⁶ S. K. Bajgain, D. B. Ghosh, B. B. Karki, Phys. Chem. Minerals **42**, 393 (2015).
- ²⁷ W.-G. Seo, F. Tsukihashi, ISIJ International, **44** 1817 (2004).
- ²⁸ W.-G. Seo, D. Zhou, F. Tsukihashi, Mater. Trans. (46), 643 (2005).
- ²⁹ T. Matsumiya, A. Nogami, Y. Fukuda, ISIJ Int. **33**, 210 (1993).
- ³⁰ L. Zhang, J. A. Van Orman, D. J. Lacks, Chem. Geol. **275**, 50 (2010).
- ³¹ M. Bouhadja, N. Jakse, and A. Pasturel, J. Chem. Phys. **138**, 224510 (2013).
- ³² M. Bouhadja, N. Jakse, and A. Pasturel, Mol. Sim., **40**, 251-259 (2014).
- ³³ M. Bouhadja, N. Jakse, and A. Pasturel, J. Chem. Phys. **140**, 234507 (2014).
- ³⁴ D. K. Belashchenko, Russ. Chem. Rev. **66**, 733 (1997).
- ³⁵ M. Huggins, J. E. Mayer, J. Chem. Phys., **1**, 643 (1933).
- ³⁶ J. Sun, A. Ruzsinszky, J. P. Perdew, Phys. Rev. Lett. **115**, 036402 (2015).
- ³⁷ B. Fultz, Prog. Mat. Sci., **55**, 247 (2010).
- ³⁸ O. Anderson, *Equations of state of solids for geophysicists and ceramic science*. (New York:

Oxford University Press, 1995).

- ³⁹ L. Kaufman and H. Bernstein, *Computer Calculation of Phase Diagrams* (Academic Press New York, 1970).
- ⁴⁰ P. Hohenberg and W. Kohn, Phys. Rev. **136**, B864 (1964).
- ⁴¹ W. Kohn and L. J. Sham, Phys. Rev. **140**, A1133 (1965).
- ⁴² G. Kresse, J. Hafner, Phys. Rev. B **48**, 13115 (1993).
- ⁴³ G. Kresse, J. Hafner, Phys. Rev. B **49**, 14251 (1994).
- ⁴⁴ G. Kresse, J. Furthmüller, Comput. Mat. Sci. **6**, 15 (1996).
- ⁴⁵ G. Kresse, D. Joubert, Phys. Rev. B, **59**, 1758 (1999).
- ⁴⁶ H. J. Monkhorst, J. D. Pack, Phys. Rev. B **13**, 5188 (1976).
- ⁴⁷ P. E. Blöchl, O. Jepsen, O. K. Andersen, Phys. Rev. B **49**, 16223 (1994).
- ⁴⁸ A. Togo, I. Tanaka, Scripta Mat., **108**, 1 (2015).
- ⁴⁹ M. Matsui, Miner. Mag. 58A, 571 (1994).
- ⁵⁰ T. K. Bechgaard, J. C. Mauro, M. Bauchy, Y. Yue, L. A. Lamberson, L. R. Jensen, M. M. Smedskjaer, J. Non-Cryst. Solids **461**, 24 (2017).
- ⁵¹ M. Bauchy, J. Chem. Phys. **141**, 024507 (2014).
- ⁵² S. J. Plimpton, J. Comp. Phys. **117**, 1 (1995); <http://www.lammps.sandia.gov>.
- ⁵³ M. Bouhadja, N. Jakse, J. Phys.: Condens. Matter **32**, 104002 (2020).
- ⁵⁴ J. R. Morris, C. Z. Wang, K. M. Ho, C. T. Chan, Phys. Rev. B **49**, 3109 (1994).
- ⁵⁵ J. F. Lutsko, D. Wolf, S. R. Phillpot, and S. Yip, Phys. Rev. B **40**, 2841 (1989).
- ⁵⁶ P. M. Agrawal, B. M. Rice, D. L. Thompson, J. Chem. Phys. **118**, 9680 (2003); *ibid.* **119**, 9617 (2003).
- ⁵⁷ N. Jakse, A. Pasturel, J. Chem. Phys. **123**, 244512 (2005).
- ⁵⁸ J. Solca, A. J. Dyson, G. Steinebrunner, B. Kirchner, H. Huber, J. Chem. Phys. **108**, 4107 (1998).
- ⁵⁹ D. R. Chang and R. A. Howard, High Temp. Sci. **15**, 209 (1982).
- ⁶⁰ [A. Erba, M. Shahrokhi, R. Moradian, R. Dovesi, J. Chem. Phys. **142**, 044114 (2015).
- ⁶¹ K. Binder and W. Kob, *Glassy Materials and Disordered Solids* (World Scientific Publishing, Singapore, 2005).
- ⁶² C. A. Angell, J. Phys. Chem. Solids **49**, 863 (1988).
- ⁶³ D. Belmonte, G. Ottonello, M. Vetuschi Zuccolini, CALPHAD **59**, 12 (2017).

⁶⁴ G. Deffrennes, N. Jakse, C. M. S. Alvares, I. Nuta, A. Pasturel, A. Khvan, A. Pisch (submitted to Calphad).